Swimming by medusae *Sarsia tubulosa* in the viscous vortex ring limit

Kakani Katija* and Houshuo Jiang

Applied Ocean Physics and Engineering, Woods Hole Oceanographic Institution, Woods Hole, Massachusetts 02543, United States of America

April 29, 2013

*corresponding author: kakani@whoi.edu

Acknowledgments

The authors would like to thank J.H. Costello for his invaluable assistance in maintaining animals at the Marine Biological Laboratory. We are very grateful for comments we received on the manuscript by S.P. Colin. We would also like to thank M. Milano for providing us with a robust Matlab fitting algorithm. Finally, we are grateful to two anonymous reviewers and A. Visser for their helpful comments on the manuscript. K.K. is supported by the Postdoctoral Scholar Program at the Woods Hole Oceanographic Institution (WHOI), with funding provided by the Devonshire Foundation and WHOI's Office of Research. H.J. is supported by a National Science Foundation grant NSF OCE-1129496 and an award from WHOI's Ocean Life Institute.

Abstract

As organisms swim in their natural environment, they are constantly striving to successfully forage, escape from predation, and search for mates to reproduce. At some stage in their life cycle, most organisms in the ocean have operated in environments where the Reynolds number (Re) is small, and have developed strategies and behaviors to overcome the effects of viscosity. Relatively little is known about these animal-fluid interactions at small ($Re > 1$), viscous size scales. Swimming organisms have been described analytically using the self-propelled swimmer model, which applies for conditions where the organism is assumed to swim steadily in a non-inertial fluid regime or $Re < 1$. However, for unsteady swimming processes, such as jumping or jet propulsion, these steady models do not take into account the impulsiveness of the swimming behavior. The unsteady impulsive Stokeslet and impulsive stresslet models have been used to describe jumping by copepods, but neither model has been applied to jetting organisms. The purpose of this study is to identify which analytical, unsteady model best describes swimming by jetting organisms at small, viscous length scales. We conducted high-speed kinematic and velocity field measurements on 1 mm velar diameter *Sarsia tubulosa*, a jetting, ambush-feeding medusae. From our measurements and comparisons using similar criteria established for copepod jumping, we conclude that the impulsive Stokeslet model more accurately describes swimming by small *S. tubulosa*. Since the hydrodynamic signature of an impulsive Stokeslet does not have strong vorticity bounding the medusa's body, this finding has important ecological implications for the ambush-feeding predator.

Keywords: *Sarsia tubulosa*, jet propulsion, impulsive Stokeslet, impulsive stresslet, viscous vortex ring

Introduction

[1] As organisms swim in their natural environment, they are constantly striving to successfully forage, escape from predation, and search for mates to reproduce (Yen and Strickler, 1996; Visser, 2001; Kiørboe, 2008). During these activities, animals are interacting with their fluid environment and they generate fluid signatures around their body and in their wake. At some stage in their life cycle, most organisms in the ocean have operated in environments where the Reynolds number (Re) is small, and have developed strategies and behaviors to overcome the effects of viscosity. Relatively little is known about animal-fluid interactions at these small size scales where $Re \sim 1$–10.

[2] A variety of analytical models have been used to describe steady swimming by small organisms in a non-inertial fluid regime (or $Re \ll 1$, Lighthill, 1975; Afanasyev, 2004). These models have been widely used to describe swimming by microorganisms and copepods, where experimental measurements of fluid signatures generated at these small size and time scales were prohibitive until recently (Guasto et al., 2012). The behavior of hydrodynamic signals generated by swimming organisms can be described by these analytical models and used to elucidate animal mechanics and ecological impact. Analytical models based on steady, Stokes flow solutions (i.e., $Re = 0$) such as a Stokeslet and stresslet, describe continuous feeding currents of plankters (e.g., copepods), where $Re \sim 1$–10 (Jiang et al., 1999; Visser, 2001; Jiang et al., 2002; Jiang and Strickler, 2007). For example, the velocity field scaling for these analytical models can be inversely proportional to some power of the radial distance r from the source of the fluid disturbance (Visser, 2001; Jiang and Kiørboe, 2011a). For a negatively buoyant hovering plankter, which is described by a steady Stokeslet (Visser, 2001), the velocity field u is inversely proportional to r or $u \sim \frac{1}{r}$. For a cruising, neutrally buoyant plankter, the flow field is described by a steady stresslet, and $u \sim \frac{1}{r^2}$. Therefore depending the behavior exhibited by the swimming organism, the spatial extent and velocity magnitude of the hydrodynamic signals change, which has implications for organismal fitness (Visser,

2001).

[3] For impulsive swimming behaviors, such as jumping, two unsteady viscous vortex ring models (an impulsive Stokeslet and impulsive stresslet) have been applied across several species of copepods (Kiørboe et al., 2010b; Jiang and Kiørboe, 2011a,b; Murphy et al., 2012; Catton et al., 2012). The impulsive stresslet model has been found to be appropriate for repositioning jumps and escape jumps of larger copepods (Jiang and Kiørboe, 2011a; Catton et al., 2012); the impulsive Stokeslet model has been shown to describe escape jumping copepods exhibiting multiple power strokes based on computational analysis (Jiang and Kiørboe, 2011b). The velocity field scales as $u \sim \frac{1}{r^3}$ and $u \sim \frac{1}{r^4}$ for the impulsive Stokeslet and impulsive stresslet models, respectively (Jiang and Kiørboe, 2011a). In other words, the velocity magnitude of the hydrodynamic signal generated by jumping copepods falls off more rapidly than for a continuously swimming or feeding organism. Therefore for smaller organisms, continuous feeding behavior has increased risk for prey trying to avoid predation (Kiørboe et al., 2010b). For copepods that generate hydrodynamic signals more akin to impulsive stresslets than impulsive Stokeslets, the flow field provides camouflage surrounding the animal's body such that a predator cannot isolate the copepod's position from the hydrodynamic signal (Jiang and Kiørboe, 2011a). Although demonstrated successfully in copepods, we would like to determine whether other impulsively swimming organisms, specifically jet propelled medusae, can be described using impulsive, viscous vortex ring models.

[4] Medusan propulsive modes are described as either rowing or jetting (Colin and Costello, 2002; Dabiri et al., 2005, 2006). A medusan swimming cycle is comprised of a contraction and relaxation phase. Rowing propulsion is characterized by slower contraction and relaxation phases (or swimming cycles), where the flow structures combine to augment propulsion (Dabiri et al., 2005). Jetting medusae swim by rapid, full-body contractions, which expels fluid from the subumbrellar cavity and results in forward momentum (Daniel, 1983; Dabiri et al., 2006). Jet-propelled medusae are able to achieve high swimming speeds, although

doing so is energetically unfavorable when compared to rowing (Daniel, 1985; Sahin et al., 2009; Dabiri et al., 2010). Interestingly, the selection of swimming modes are strongly correlated with feeding behavior and morphological characteristics (Colin and Costello, 2002; Colin et al., 2003; Costello et al., 2008). Therefore, despite utilizing an inefficient mode for swimming, jetting medusae remain motionless most of the time and forage as ambush predators (Colin and Costello, 2002; Colin et al., 2003).

[5] Numerous studies have been conducted to understand the animal-fluid interactions medusae encounter throughout development (McHenry and Jed, 2003; Weston et al., 2009; Blough et al., 2011; Herschlag and Miller, 2011). As adults, medusae occupy fluid regimes where Reynolds numbers vary from 100–1000, and inertial forces dominate. Medusan ephyrae bud at length scales on the order of 1 mm, and swim in fluid regimes where viscous forces cannot be neglected ($Re \sim 10$). Viscosity has been shown to profoundly alter the boundary layer dynamics and swimming ability of rowing medusae (Feitl et al., 2009), however little is known about these dynamics for small ($\sim$1 mm velar diameter), jetting medusae. Although observations of jetting medusae have relied on the use of dye visualization and particle tracking to describe swimming kinematics (Colin and Costello, 2002; Weston et al., 2009; Blough et al., 2011), little is known about jetting propulsive performance. Due to the challenges associated with capturing fluid motions at small length and time scales, there is a limited body of literature devoted to measurements of the hydrodynamic signals and energetics of jetting organisms in general (Bartol et al., 2009).

[6] Like copepods, jetting medusae generate thrust quickly by accelerating fluid on fast time scales (Daniel, 1983; Colin et al., 2003; Dabiri et al., 2006). Fluid expelled from the subumbrellar cavity of a medusa generates a toroidal vortex ring, a structure that is also present in jumping copepod wakes (Kiørboe et al., 2010b; Jiang and Kiørboe, 2011b; Murphy et al., 2012). Therefore, we expect that the unsteady analytical models used to describe copepod jumping can be used to describe swimming by small, jetting medusae. The purpose

of this study is to identify which analytical model best describes swimming by jetting medusae at small size scales. We conducted digital particle image velocimetry (DPIV; Adrian, 1991; Willert and Gharib, 1991) measurements with high frame rates to characterize the wakes generated by ∼1 mm velar diameter *Sarsia tubulosa* (M. Sars, 1835), a species of jellyfish that swims using jet propulsion throughout their life cycle. Using this data, we compare the ability of two analytical viscous vortex ring models (the impulsive Stokeslet and the impulsive stresslet model) to describe the resultant hydrodynamic signature using criteria established for jumping copepods (Jiang and Kiørboe, 2011b). From our measurements and analysis, we conclude that the impulsive Stokeslet model more accurately describes swimming by small *S. tubulosa*.

Analytical Methods

[7] As mentioned previously, the impulsive Stokeslet and impulsive stresslet models have been recently used to describe swimming modes and jumping behaviors of copepods. Neither model has been applied to similarly-sized jetting organisms, such as squid paralarvae and small jellyfish, where the time scales of thrust generation and Re range are consistent with impulsive copepod repositioning jumps ($Re \sim 10$). Therefore, one would expect that the impulsive Stokeslet and impulsive stresslet models can also be used to describe swimming by small (∼1 mm velar diameter), jetting medusae.

[8] When a jetting medusa swims, each muscular contraction results in the expulsion of fluid from the body cavity of the animal, which creates a vortex ring in its wake (Fig. 1A). The vortex ring in the wake can also be represented by a compact region of vorticity (Fig. 1B). In addition, as the body moves, a compact region of opposite-signed vorticity is generated near the surface of the animal's body. The impulsive Stokeslet model replaces the wake flow generated by the jetting animal with a point momentum source applied in the direction

opposite to its direction of motion (Fig. 1C). The impulsive stresslet model differs from the impulsive Stokeslet model in that the overall flow is replaced with two point momentum sources directed away from each other in order to represent (assumed) equal contributions of wake vorticity and body-bound vorticity due to the jetting process (Fig. 1D). Therefore, the major difference between the two impulsive, unsteady models is the relative contribution of the body-bound vorticity to the fluid signature generated by the swimming organism.

[9] Based on a preliminary visual examination of flow patterns generated by small *Sarsia tubulosa*, the apparent lack of body-bound vorticity during swimming suggests that an impulsive Stokeslet rather than an impulsive stresslet more accurately represents the flow field. To statistically determine whether one impulsive model over another describes swimming by small, jetting medusae, we utilize two tests that are based on the comparison of swimming kinematic data and the hydrodynamic signal (fluid circulation and separation of vortical flow features) generated by their swimming. These tests are described in more detail in the following sections, and derivations of related quantities can be found in Kiørboe et al. (2010b) and Jiang and Kiørboe (2011a,b). Results from these two tests will be used to inform whether an impulsive Stokeslet or impulsive stresslet model can describe small, jetting organisms.

Test 1: Measured vs. Fitted Strengths of the Impulsive Stokeslet and Impulsive Stresslet

[10] To determine whether flows generated by ∼1 mm velar diameter *Sarsia tubulosa* can be accurately represented by a theoretical solution for viscous vortex rings, we first compare measured quantities representing the animal's kinematics to the behavior of the wake structures generated by the swimming organisms. In other words, we can use dimensional analysis to characterize the strength of the impulsive Stokeslet or impulsive stresslet ($I_{measured}$ or $M_{measured}$), and compare these quantities with fitted trends based on the viscous decay of fluid circulation in the animal's wake (I_{fitted} or M_{fitted}; Jiang and Kiørboe, 2011b).

[11] The time-varying circulation (Γ) for an impulsive Stokeslet can be written in terms of the strength of the impulsive Stokeslet (I, with units $\mathrm{m}^4\ \mathrm{s}^{-1}$) as

$$\Gamma_{Stokeslet}(t) = \frac{I}{4\pi\nu t}, \tag{1}$$

where ν is the kinematic viscosity and t is time. By fitting the decay of measured circulation such that $\Gamma_{measured}(t) = A_I \left[\nu\left(t - t_{0,1}\right)\right]^{-1}$, where A_I is a fitting parameter (with units $\mathrm{m}^4\ \mathrm{s}^{-1}$) and $t_{0,1}$ is a virtual time origin (another fitting parameter), and solving for I in Eq. 1 to find I_{fitted}, we find that

$$I_{fitted} = 4\pi A_I. \tag{2}$$

The analytical solution described by Eq. 1 is for the flow starting from a singularity. Thus, when fitting the measured circulation data to Eq. 1, a virtual time origin ($t_{0,1}$) has to be included.

[12] Using dimensional analysis, a measured quantity that characterizes the strength of the assumed impulsive Stokeslet-like *S. tubulosa* wake flow field ($I_{measured}$) can be defined as

$$I_{measured} = V\,U_{max}, \tag{3}$$

where V is the animal body's volume (assumed to be a hemi-spheroid) and U_{max} is the maximum swimming speed over a swimming cycle.

[13] The circulation for an impulsive stresslet is

$$\Gamma_{stresslet}(t) = \frac{M}{8\pi^{3/2}\left(\nu t\right)^{3/2}}, \tag{4}$$

where M is the strength of the impulsive stresslet with units of $\mathrm{m}^5\ \mathrm{s}^{-1}$. By fitting the decay of the circulation such that $\Gamma_{measured}(t) = A_M \left[\nu\left(t - t_{0,2}\right)\right]^{-3/2}$, where A_M is a fitting parameter

(with units $m^5\ s^{-1}$) and $t_{0,2}$ is a virtual time origin (another fitting parameter), and solving for M in Eq. 4, we find the following expression for M_{fitted},

$$M_{fitted} = 8\pi^{3/2} A_M. \tag{5}$$

The analytical solution described by Eq. 4 is for the flow starting from a singularity. Thus, when fitting the measured circulation data to Eq. 4, a virtual time origin ($t_{0,2}$) has to be included.

[14] Finally, from dimensional analysis, a measured quantity that characterizes the strength of the assumed impulsive stresslet-like *S. tubulosa* flow field ($M_{measured}$) can be defined as

$$M_{measured} = U_{max}\, V\, D_{travel}, \tag{6}$$

where D_{travel} is the distance traveled by the animal over a single swimming cycle. The travel distance D_{travel} is chosen as the relevant length scale because the travel distance naturally sets the upper limit of the separation distance between the force application points of the two instantaneous, opposite momentum sources (i.e., the impulsive stresslet).

[15] These propulsion-related bulk parameters, such as maximum swimming speed (U_{max}), travel distance (D_{travel}), and animal body volume (V) should control the behavior of the propulsion-induced flow field. Heuristically, a fitted strength (i.e., I_{fitted} or M_{fitted} or both, derived from the propulsion-induced flow field) should be linearly related to the corresponding measured strength ($I_{measured}$ or $M_{measured}$, derived from the propulsion-related bulk parameters). Therefore, if the degree of linearity for the impulsive Stokeslet (i.e., $I_{fitted} = C_1\, I_{measured}$, where C_1 is a fitting constant) is greater than for the impulsive stresslet (i.e., $M_{fitted} = C_2\, M_{measured}$, where C_2 is a fitting constant), the jetting medusa is better represented by an impulsive Stokeslet.

[16] To determine relative linearity of the viscous vortex models, we calculate the regression through the origin (R^2) for both the impulsive Stokeslet and impulsive stresslet data using the definition

$$R^2 = \frac{\sum_i^N \hat{Y}_i^{\,2}}{\sum_i^N Y_i^2}, \tag{7}$$

where $\hat{Y}_i$ is the ith value of the linear model and Y_i are the measured values (Turner, 1960; Eisenhauer, 2003). The viscous vortex ring model whose R^2 value is closest to 1 more accurately describes swimming by $\sim$ 1 mm velar diameter *S. tubulosa*.

Test 2: Separation of Velocity Stagnation Points and Vorticity Singularities

[17] A characteristic feature of viscous vortex rings generated by an impulsive momentum source is that the position of the vorticity maximum and minimum, and the velocity stagnation points separate over time. Fig. 2 shows a representative $\sim$1 mm velar diameter *S. tubulosa* (data set 111129–2) velocity (A, white vectors) and vorticity (B, white contours) field with stagnation points and vorticity maximum and minimum indicated by the asterisks. The velocity and vorticity fields correspond to 0.52 s after the start of the contraction phase and near the start of the relaxation phase. In the inviscid vortex ring limit, the separation of the positions of the velocity stagnation points and maximum and minimum vorticity remains constant over time. However, in the viscous vortex ring limit, the positions of these points diverge over time, resulting in an increasing separation distance. As shown in Fig. 2, the position of the velocity stagnation points and the vorticity maximum and minimum do not coincide. An analytical solution for the separation distance of these points [$\Delta(t)$] for an impulsive Stokeslet and impulsive stresslet model is

$$\Delta(t) = \begin{cases} 1.61\sqrt{\nu t} & \text{for an impulsive Stokeslet,} \\ 1.30\sqrt{\nu t} & \text{for an impulsive stresslet.} \end{cases} \tag{8}$$

The observed separation distance between the vorticity maximum and minimum and the velocity stagnation points can be fitted by $\Delta(t) = A_{sep}\sqrt{\nu\,(t - t_0)}$, where A_{sep} is a dimensionless fitting constant and t_0 is a virtual time origin (another fitting constant). Comparing the value of A_{sep} with the value of the constant in Eq. 8, we can determine whether the flow generated by small, ∼1 mm diameter *S. tubulosa* is represented best by an impulsive Stokeslet or impulsive stresslet.

Experimental Methods

[18] *Sarsia tubulosa* were cultured in filtered, chilled seawater (temperature at 10 °C and salinity of 35 ppt, density and viscosity corresponds to $\rho = 1026.95\,\mathrm{kg\,m^{-3}}$ and $\nu = 1.354 \times 10^{-6}\,\mathrm{m^2\,s^{-1}}$) at the Marine Biological Laboratory in Woods Hole, Massachusetts. Measurements of swimming *S. tubulosa* (M. Sars, 1835) began in Fall of 2010 and ended in Winter of 2011. Multiple *S. tubulosa* with velar diameters ranging from 1 to 4 mm were placed in a rectangular glass filming vessel with outer dimensions of 5 cm W ×10 cm H ×4 cm D, and 10 μm glass beads were added to the tank for seeding visualization. During measurements, the filming vessel was partially submerged in an ice bath so as to maintain fluid temperatures near 10 °C. Measurements concluded when a glass thermometer (placed in the filming vessel) would read 13 °C. The filming vessel would then be refilled with 10 °C seawater, glass particles would be added, and flow measurements would resume.

[19] Animal swimming motions were captured using a high-speed camera (Fastcam SA3, Photron), 100 mm lens (Carl Zeiss, Inc.), and extension tubes to yield viewing areas on the order of 1 cm^2. Illumination was provided by a 300 W, 808 nm near-infrared laser (Firefly, Oxford Lasers), and built-in optics generated a light sheet 0.5 mm thick. In order to resolve the high-speed, short duration flows generated by medusae, images were captured at 1000 fps at full, 1024 pixels × 1024 pixels resolution. Data sets where the body (indicated by the

laser sheet intersecting the manubrium) and propulsive wake were bisected by the laser sheet within the camera's field of view before, during, and after the swimming cycle were used for subsequent analysis.

[20] Raw particle images were used to determine *S. tubulosa* kinematics parameters using an in-house Matlab image processing code. From consecutive images, we extracted *S. tubulosa*'s relaxed velar diameter, body diameter (D), body height (H), duration of swimming cycle (including the time of contraction and relaxation phase), and the distance traveled during one swimming cycle. The body volume (V_b) of the medusa was calculated based on the shape of a prolate, hemi-spheroid, $V_b = \frac{2}{3}\pi\left(D/2\right)^2 H$. The swimming speed was computed using finite differencing and data was smoothed (using a Savitzky-Golay filter) using Matlab. The characteristic length and velocity scales used to determine the Reynolds number (Re) correspond to the relaxed velar diameter and the maximum swimming velocity, respectively. Although data were collected for animals ranging in size, we present data for 11 separate swimming cycles of $\sim$1 mm velar diameter *S. tubulosa*.

[21] Velocity fields were calculated with DaVis (LaVision), a digital particle image velocimetry (DPIV; Adrian, 1991; Willert and Gharib, 1991) software package, using a multi-pass algorithm with initial and final interrogation window sizes of 64 pixels $\times$ 64 pixels (0.5 mm $\times$ 0.5 mm) and 32 pixels $\times$ 32 pixels (0.3 mm $\times$ 0.3 mm), respectively, with a 50% overlap. To minimize the effect of the body, an evolving, algorithmic mask was defined within DaVis. Before smoothing data, the velocity vectors whose corresponding interrogation windows overlapped the mask by 20% were removed. For discussions related to the body-bound vorticity, the masked and smoothed velocity field data were used. Calculations of fluid circulation in the wake of *S. tubulosa* used unmasked and smoothed velocity field data since the decay phase of fluid circulation occurs towards the end of the muscular contraction phase; the vortex ring is completely separated from the body and hence the effect of body bound vorticity on circulation of the detached viscous vortex ring is negligible. Velocity field

data were exported from DaVis and additional post-processing steps (discussed below) were conducted in Matlab.

[22] Using the velocity and vorticity fields, and an in-house Matlab code, the time-varying positions of the fluid stagnation points (defined to be where the magnitude of velocity within the jet is equal to zero) and the maximum and minimum locations of vorticity within the jet were found. To minimize the effect of a coarse mesh from the DPIV analysis, the tracking of these points was improved by interpolating the position and velocity meshes in Matlab. Since there are two stagnation points and a maximum and minimum vorticity location, two values of separation were averaged for each time step. The separation of fluid stagnation points and maximum/minimum vorticity were fitted with a square root function using a robust fitting algorithm in Matlab.

[23] By assuming that the medusan wake is axisymmetric, we can fully characterize interesting fluid dynamics quantities (i.e., wake kinetic energy, circulation, impulse, etc.) using planar measurement techniques. For an axisymmetric flow, the time-varying fluid circulation $\Gamma(t)$ can be found from the vorticity field ω by

$$\Gamma(t) = \iint_S \omega(t) \cdot d\mathbf{S} \approx \sum_S \omega(x, r, t)\, \Delta S, \tag{9}$$

where S is an arbitrary surface bounded by a closed contour surrounding the non-zero (positive or negative) vorticity field and ΔS corresponds to the velocity field grid mesh spacing. An in-house Matlab code was used to compute the circulation in the wake of swimming *S. tubulosa*. Total time-varying circulation is computed by averaging the two values of circulation (determined from the positive and negative vorticity areas) representing the regions S on either side of the rotational axis. Once the circulation is computed for each data set, the decay of circulation is fitted to a specified function using the aforementioned fitting algorithm in Matlab. The values from the fit are then used to compute I_{fitted} and M_{fitted} and compared

with the measured values ($I_{measured}$ and $M_{measured}$) to determine whether the flow fields can be represented by an impulsive Stokeslet or impulsive stresslet.

Results

[24] For a representative swimming cycle of ∼1 mm velar diameter *Sarsia tubulosa* (data set 111129-2), we see the correspondence between velar diameter (black line, left vertical axis), bell height (black dotted line, left vertical axis), and swimming speed (dark gray line, right vertical axis), where Fig. 3 shows the smoothed data. As the muscles surrounding the bell orifice contract (the velar diameter is reduced), the medusa elongates the height of its bell, and the swimming speed increases. The maximum bell height occurs nearly at the same instant when the minimum velar diameter is achieved (at $t = 0.08$ s). However, there is a time delay between reaching the maximum swimming speed (at $t = 0.06$ s) and when the relaxation period starts at $t = 0.08$ s. Before the end of contraction, the medusa rapidly decelerates and continues to decelerate during the relaxation phase. Towards the end of the relaxation phase, however, the rate of deceleration slows down, and a swimming speed near 9.5 mm s^{-1} is maintained for nearly 0.03 s before decelerating again. This feature of the medusan swimming speed during the relaxation phase was consistently present in all 11 data sets of ∼1 mm velar diameter *S. tubulosa*.

[25] Averaging each animal's maximum swimming speed yields a value of 18 mm s^{-1}, nearly 20 times the length of the velar diameter traveled per second (Table 1). The distance traveled over a swimming cycle is slighter greater than the velar diameter in some cases and nearly a factor of 3 larger in others, yielding an average distance of 1.9 mm per swimming cycle. In most cases, the data sets with higher maximum speeds correspond to the furthest distance traveled. The average Re is 15 for the ∼1 mm velar diameter size scale.

[26] The velocity and vorticity fields generated over a swimming cycle are very different in ∼1 mm velar diameter viscous range (Fig. 4) versus those commonly seen in higher Re cases (Lipinski and Mohseni, 2009; Dabiri et al., 2010; Herschlag and Miller, 2011). The first frame shows the fluid disturbance generated at the initiation of the contraction phase. For the ∼1 mm *S. tubulosa*, the second frame corresponds to the end of the contraction phase where a vortex ring is clearly present. The third frame reveals the fluid disturbance midway through the relaxation phase; fluid is being pulled into the subumbrellar cavity of the medusa and strong vorticity with opposite rotational sense of the vortex ring in the wake is present. In addition, an elongated vortex ring is present in the wake of the ∼1 mm medusa. The final frame (Fig. 4, top row) shows the fluid disturbance at the end of the relaxation phase, nearly 0.19 s after the initiation of the swimming cycle. The velocity and vorticity fields are quickly diffused and are nearly the same magnitude as the background flow. In addition, the magnitude of the body bound vorticity is less than that due to the wake vortex throughout the swimming cycle.

[27] From the time-varying velocity and vorticity fields (in Fig. 4) and using Eq. 9, the time varying fluid circulation (Γ) in the wake of swimming *S. tubulosa* can be determined. The fluid circulation (black dots, left vertical axis; data set 101117–4) is plotted with the animal's smoothed time-varying velar diameter (gray line, right vertical axis) in Fig. 5. The plotted fluid circulation is the average of two values of circulation derived from the positive (right side of the vortex ring) and negative (left side of the vortex ring) vorticity fields as shown in Fig. 4. The maximum circulation is achieved at the end of the contraction phase, and values of circulation decay soon afterward. A curve representing the solution of an impulsive Stokeslet (dashed gray line) is fitted using the circulation data during the decay phase only. The error bars represent the standard deviation between both values of fluid circulation derived from the positive and negative values of vorticity in the wake of *S. tubulosa*. The fluid circulation starts decaying rapidly at the end of the contraction phase. The fitting constants (I_{fitted} and M_{fitted}) for the impulsive viscous vortex ring models are

determined by fitting the decay phase of the fluid circulation data.

[28] The values for $I_{measured}$, I_{fitted}, $M_{measured}$, and M_{fitted} were found for all 11 data sets of ∼1 mm velar diameter *S. tubulosa*. The values for $I_{measured}$ and $M_{measured}$ are determined by assuming that the medusa's body volume can be approximated by a hemi-spheroid. These results are summarized in Table 2. The root mean squared error (RMSE) values in columns 4 and 7 (Table 2) show the goodness of fit of the impulsive Stokeslet and impulsive stresslet model (Table 2, columns 4 and 7, respectively) to the decay of fluid circulation. The values representing the strength of the impulsive Stokeslet (I) and the strength of the impulsive stresslet (M) are plotted in Fig. 6 in the top and bottom panel, respectively. The measured and fitted values of the impulsive Stokeslet strength for all 11 data sets show stronger agreement ($R^2 = 0.93$) than the measured and fitted values for the strength of the impulsive stresslet ($R^2 = 0.65$). Since the measured and fitted data for the impulsive Stokeslet model has greater linearity than the impulsive stresslet model (Test 1), preliminary findings suggest that these flow fields may be more accurately described by an impulsive Stokeslet.

[29] Fig. 7A shows the position of the vorticity maximum and minimum (circles) and the velocity stagnation points (asterisks) in the wake of a ∼1 mm velar diameter animal over time. At the start of the swimming cycle, these points overlap; as time progresses, the position of these points separate. The separation of the velocity stagnation points and vorticity maxima and minima over time is plotted in Fig. 7B. Since there are two separating pairs of points, the data in Fig. 7B are the averaged values of separation over time. A square root ($A_{sep}\sqrt{t - t_0}$; solid black line) are fitted to the ∼1 mm velar diameter (Fig. 7B) data for comparison. Fitting the point separation data to a square root function for each data set yields an average value for the separation coefficient A_{sep} (Eq. 8) as 1.67 (Table 2). The goodness of fit is confirmed by low RMSE values (Table 2, column 9), thereby enhancing our confidence in the fitted values of A_{sep}. Therefore, comparing A_{sep} (determined by fitting the experimental separation data) with the theoretical value based on the viscous vortex ring

model (Test 2; see Eq. 8), these data are more accurately described by an impulsive Stokeslet.

Discussion

Evaluating test results: impulsive Stokeslet vs. impulsive stresslet model

[30] Based on the visual examination of flow patterns generated by ∼1 mm velar diameter *Sarsia tubulosa* (Fig. 4), the apparent lack of body-bound vorticity during jetting propulsion suggests that an impulsive Stokeslet rather than an impulsive stresslet more accurately represents the flow field. We utilized two tests to statistically determine which impulsive viscous vortex ring model more accurately describes the hydrodynamic disturbance induced by a jetting medusae. Close evaluation of the proposed tests shows that the impulsive Stokeslet model better describes the flow generated by ∼1 mm velar diameter *S. tubulosa* than the impulsive stresslet model. In Test 1, the decay of fluid circulation is fitted to a theoretical solution for each model (Eqs. 1 and 4) to find the strengths of the impulsive Stokeslet and stresslet (I_{fitted} and M_{fitted}, respectively). The fitted line of the circulation decay for the impulsive Stokeslet (dashed, gray line; Fig. 5) shows good agreement between the data and the theoretical solution. From the RMSE values of the nonlinear fit of fluid circulation (see Table 2, columns 4 and 7), the goodness of fit is equally as good for the impulsive stresslet and Stokeslet, enhancing our confidence in the fitted values of I_{fitted} and M_{fitted}, respectively.

[31] Using dimensional analysis (Eqns. 3 and 6), we find values for the impulsive Stokeslet and the impulsive stresslet strength ($I_{measured}$ and $M_{measured}$, respectively) based on the organism's swimming characteristics: body volume, maximum swimming speed, and travel distance over a swimming cycle. These parameters were selected because they best represented the physical parameters of swimming in viscous length and time scales. The measured quantities ($I_{measured}$ and $M_{measured}$) are directly compared with the fitted quantities (I_{fitted} and M_{fitted}) and a linear fit is generated from the data (thick black line; Fig. 6). The viscous

vortex ring model that has the better linear correspondence between measured and fitted strengths will best represent swimming by ∼1 mm velar diameter *S. tubulosa*. To determine the degree of linearity of measured and fitted quantities, we quantify the correlation coefficient (R^2, equation 7) for the impulsive Stokeslet and stresslet model as 0.93 and 0.65, respectively. Preliminary results of Test 1 would support the finding that the impulsive Stokeslet model more accurately describes the flow generated by swimming *S. tubulosa* with ∼1 mm velar diameters.

[32] Upon closer inspection of Fig. 6A, two data points corresponding to the same organism (data sets 101121–1a and 101121–1b) can be viewed as outliers, with most of the data points clustered between $I_{measured} = 0.15 - 0.45 \times 10^{-13}$ m^4 s^{-1}. The same two data sets may also be viewed as outliers for the impulsive stresslet strength (where $M_{measured} > 1.5 \times 10^{-13}\mathrm{m}^5\mathrm{s}^{-1}$) in Fig. 6B. To be sure, these data points are not the only data that could be interpreted as outliers in Fig. 6B. By neglecting data sets 101121–1a and 1b and refitting the data, the resultant correlation coefficients for the linear fit of impulsive Stokeslet and stresslet models improve to 0.95 and 0.73, respectively. Although the difference in R^2 between both models are reduced when removing potential outliers, we conclude that the flow fields are better represented by an impulsive Stokeslet based on Test 1 only.

[33] Test 2 evaluates the separation characteristics between vorticity maxima and minima from velocity stagnation points in the wake of swimming *S. tubulosa*. The separation of these points over time are fitted to $A_{sep}\sqrt{\nu\,(t - t_0)}$, where A_{sep} and t_0 are fitting parameters. The goodness of fit is confirmed by RMSE values that are three to four orders of magnitude less than the separation values (see column 9 of Table 2), thereby enhancing our confidence in the fitted values of A_{sep}. Values of A_{sep} for ∼1 mm velar diameter *S. tubulosa* (Table 2, column 8) yield an average value of 1.67, which is near the theoretical limit for the impulsive Stokeslet ($A_{sep} = 1.61$), and is much larger than the value for the impulsive stresslet model ($A_{sep} = 1.30$). Therefore, Test 2 finds that swimming by ∼1 mm velar diameter *S. tubulosa*

is better described by an impulsive Stokeslet model.

Impulsive Stokeslet model describes swimming for small, jetting medusae

[34] As previous work on copepod jumping has shown (Kiørboe et al., 2010b; Jiang and Kiørboe, 2011b,a), the impulsive dynamics of copepod jumping behavior are not adequately represented by steady viscous vortex models. We find that the decay of fluid structures and kinematic behavior of ∼1 mm velar diameter jetting medusae *S. tubulosa* is very similar to the results shown for jumping copepods, where steady viscous models do not apply. Based on our experimental study and careful evaluation of analytical tests, we show that the flow generated by ∼1 mm velar diameter *S. tubulosa* was best described by the impulsive Stokeslet model, which is characterized by a strong region of vorticity in the wake with negligible body-bound vorticity.

[35] The magnitude of body-bound vorticity is much less than vorticity associated with the wake vortex (Fig. 4, $t = 0.065$ s). This difference in vorticity may be attributed to the kinematic swimming behavior and is discussed below. For jumping copepods undergoing repositioning hops, a strong body-bound region of vorticity is ecologically beneficial due to the hydrodynamic camouflage it provides from other predators (Jiang and Kiørboe, 2011b). A predator searching for copepods would detect the same fluid signature for a vortex ring in the wake and the vorticity bounding the body, and would be unable to distinguish between them. This fluid signal, represented by an impulsive stresslet, would be ecologically beneficial to small organisms trying to avoid predation (Jiang and Kiørboe, 2011b). However, in the case of jetting, ambush feeding *S. tubulosa*, a strong region of vorticity (or shear deformation) surrounding its body would alert prey to its presence, eliciting prey escape responses for predator avoidance. For jetting medusae, whose hydrodynamic signal is described by an impulsive Stokeslet, it would be ecologically beneficial for them to swim from one region to

the next virtually undetected so as to lie in wait for prey.

[36] Despite the effects of viscosity, small *S. tubulosa* are able to achieve swimming speeds as high as 20 velar diameters per second with an average Reynolds number of 15 (summarized in table 1). As our data show, high swimming speeds correspond to larger travel distances of jetting medusae. Experimental results indicate that ∼1 mm velar diameter *S. tubulosa* travel up to 3 mm from the initiation of muscular contraction until the medusa's body is again stationary. Computational models of swimming by *S. tubulosa* show that after four swimming cycles, the distance traveled is between 4 and 5 body diameters (Herschlag and Miller, 2011), which is consistent with our experimental data. Larger travel distances as a result of jetting are ecologically beneficial for jetting medusae, since they result in greater separation between the body of an ambush-feeding predator and the propulsive vortex ring generated in its wake that may elicit prey escape responses.

Impulsively swimming (jetting) medusae and (jumping) copepods

[37] Table 3 summarizes average impulsive swimming characteristics that include both repositioning and escape jumping behavior of five different species of copepods (*Oithona davisae*, *Acartia tonsa*, *Calanus finmarchicus*, *Euchaeta rimana*, and *Euchaeta elongata*) and ∼1 mm velar diameter *S. tubulosa*. Instances where the copepod had multiple jumps in a single escape event (indicated by "escape, mult." entry in the second column of Table 3) are also included (Jiang and Kiørboe, 2011b; Murphy et al., 2012). These data are organized by species and body size, where the length scale corresponds to the velar diameter and the prosome length for the medusae and copepods, respectively. Studies where the fluid circulation and impulsive vortex ring model were not studied are also included (Kiørboe et al., 2010a) to understand the effects of body kinematics on swimming performance. Unless denoted by a double asterisk, data for body kinematics and hydrodynamics were acquired experimentally.

[38] For similarly sized copepods, longer power stroke durations (t_{stroke}, equivalent to contraction time in medusae) correspond to escape jumps that comprised of multiple leg beats. For the same swimming behavior, the power stroke duration roughly increases with increasing copepod size. However, when considering the power stroke duration of *S. tubulosa*, t_{stroke} is nearly an order of magnitude larger than a copepod in the same size range. Since the propulsion dynamics between medusae and copepods are dissimilar (i.e., jet propulsion via expulsion of fluid from a contracting bell versus jumping by impulsively beating metachronal legs, respectively), similarly sized medusae will not exhibit the same power stroke duration as copepods. Except for *C. finmarchicus*, the maximum swimming speed (U_{max}) varies inversely with stroke duration, and confirms previous findings (Kiørboe et al., 2010a; Jiang and Kiørboe, 2011b). In addition, given similar power stroke durations, the maximum swimming speed attained by the organism increases with increasing length scale. Due to lower acquisition frame rates, we suspect that the maximum swimming speeds of *C. finmarchicus*, *E. rimana*, and *E. elongata* (Murphy et al., 2012; Catton et al., 2012) should be larger than reported. Subsampling of data at frame rates less than 1000 fps for impulsive swimming behavior will also affect results for power stroke duration.

[39] The strength of hydrodynamic signals generated by small, jetting medusae are comparable to signals created by different species of copepods, thereby further shielding their presence from prey. The values of maximum fluid circulation achieved in the wake of jetting *S. tubulosa* (Γ_{max} = 112 mm^2 s^{-1}) are consistent with earlier measurements of wake signatures generated by 2–3 mm copepods ($\Gamma_{max} \approx 100$ mm^2 s^{-1} for *C. finmarchicus* and *E. elongata*; Jiang and Kiørboe, 2011b; Catton et al., 2012). In addition, the values for the fitted impulsive Stokeslet strength (I_{fitted}) for the ~1 mm velar diameter medusae cases range from 27 to 65 mm^4 s^{-1} compared to computational fluid dynamics estimates of 19 to 2116 mm^4 s^{-1} for *A. tonsa* and *C. finmarchicus* (Jiang and Kiørboe, 2011b). Despite the different vortex generation characteristics between jumping copepods and jetting medusae, the resulting fluid dynamics in the propulsive wakes of these organisms are comparable.

[40] There appears to be a distinct relationship between prosome length of a copepod and fluid circulation generated in their wake (Γ_{max}), which confirms the conclusions of Murphy et al. (2012). However, this argument breaks down when including *S. tubulosa*. Although smaller than *C. finmarchicus*, *E. rimana*, and *E. elongata*, *S. tubulosa* generates higher values for Γ_{max} than what has been reported for all repositioning and escape jumping copepods. We suspect that the longer stroke duration and different vortex formation process utilized by medusae results in larger fluid circulation values. As mentioned previously, jetting medusae expel fluid from their subumbrellar cavity by contracting circumferential muscles around the bell; jumping copepods generate locomotion by quickly paddling metachronal legs. We can relate the two swimming mechanisms by using dimensional analysis, where fluid circulation scales as $\Gamma \sim u^2 t$, where t corresponds to the power stroke duration t_{stroke} and velocity scale u. Therefore, since the power stroke duration of *S. tubulosa* is longer than for copepods, this scaling results in comparable values for Γ_{max}.

[41] The major hydrodynamic difference between a repositioning jump and an escape jump in copepods is the emergence of an elongated region of vorticity that is shed behind the body after the wake vortex travels away from the moving copepod (Jiang and Kiørboe, 2011b). This feature was not pronounced in the experimentally measured flow fields generated by escape jumping (with multiple leg beats) *C. finmarchicus*, where the absence of the elongated region of vorticity was largely attributed to rotation and asymmetric motion of the copepod's body (Murphy et al., 2012). However, in our studies of jetting *S. tubulosa*, we do not observe this feature in the wake of medusae whose bodies lack rotation during swimming. We suspect that the difference in hydrodynamic signatures are due to the vortex formation process utilized by these organisms. Additional metachronal legs generate smaller signatures behind the body after the initiation of the escape jump, which dissipate quickly and leaves behind an elongated region of vorticity (Jiang and Kiørboe, 2011b). Therefore, this elongated flow feature may only be present in straight, escape jumping copepods.

Factors dictating the continuum of vortex ring models

[42] As discussed earlier, there are many factors that dictate the flow fields generated by impulsively swimming organisms, with body size and power stroke duration playing a major role. Differing body kinematics between medusae and copepods may also alter flow fields. Recall that the body bound vorticity surrounding *S. tubulosa* is much lower in magnitude than the wake vorticity (Fig. 4). This difference in vorticity may be partly attributed to the kinematic behavior of ∼1 mm velar diameter *S. tubulosa*. Roughly 0.2 s before the end of bell contraction (Fig. 3), the swimming speed reaches a maximum. Although fluid is still being expelled from the subumbrellar cavity, the resultant propulsive force is overcome by viscous forces on the body, and the swimming speed begins to decrease. However, the velar diameter continues to decrease and the bell height continues to increase (Fig. 3), resulting in a more streamlined body planform. Streamlining of a body may result in a smaller boundary layer and hence a lower magnitude of body-bound vorticity. The organism continues to coast in this streamlined configuration for nearly 0.02 s before initiating the relaxation phase. Copepods cannot dynamically change their body shapes (aspect ratio of ∼0.37 for *Acartia tonsa* Kiørboe et al., 2010a) to the degree that medusae are capable (aspect ratio ranging from 0.82 to 0.41 for *S. tubulosa*), preventing them from streamlining their bodies and further modulating body-bound vorticity. Although the aspect ratio for *A. tonsa* is less than *S. tubulosa*, we suspect that the dynamic effect of drag reduction by streamlining lowers the magnitude of body-bound vorticity relative to vorticity in the wake, a characteristic of an impulsive Stokeslet. To be sure, further analysis is required to determine the relative importance of this effect on the hydrodynamics of swimming bodies.

[43] Although dynamic drag reduction of swimming medusae may play a role in dictating the flow field generated by impulsively swimming organisms, a physical explanation based on power stroke duration, jump distance, and body size is more easily supported. An impulsive stresslet consists of two simultaneously applied impulsive Stokeslets that are separated by a

short distance (ϵ, Fig. 1). As the distance between the impulsive Stokeslets in an impulsive stresslet are increased, we hypothesize that the flow field evolves in a temporally separated way as two impulsive Stokeslets. Therefore, (1) if the jump distance is larger than the body length scale L and (2) if the power stroke duration is longer than L/U, where U is the maximum swimming speed, the distance between the impulsive Stokeslets in a stresslet is increased. The wake flow field becomes less influenced by the flow field surrounding the moving body and becomes more akin to an impulsive Stokeslet only. In other words, for an impulsive stresslet to apply, the organism's jump distance needs to be small and the power stroke duration needs to be brief.

[44] As discussed earlier (refer to Table 3), repositioning jumps have the shortest power stroke duration and are often described by an impulsive stresslet model (Jiang and Kiørboe, 2011a,b). *O. davisae* undergoing a repositioning jump travels the shortest distance out of all reported jumps (Table 3; Jiang and Kiørboe, 2011a). Escape jumps have longer power stroke durations, and are often described by an impulsive Stokeslet model (current manuscript and Jiang and Kiørboe, 2011b), where the distance traveled during escape jumping is larger than repositioning jumps. Escape jumps with multiple leg beats result in higher power stroke durations and travel distances (Jiang and Kiørboe, 2011a; Murphy et al., 2012). Based on our above hypothesis, the flow field generated by *C. finmarchicus* during an escape jump with multiple leg beats should more closely resemble an impulsive Stokeslet. Although experimental results of an escape jumping (with multiple leg beats) *C. finmarchicus* has been associated with an impulsive stresslet (Murphy et al., 2012), we suspect that the rotational and asymmetric swimming behavior of the copepod altered the flow field significantly. To be sure, the scaling proposed above is applicable to straight, axisymmetric, impulsive swimming behavior.

[45] As organism size, travel distance, and power stroke duration increase, wake vortex rings begin to resemble classical inviscid vortex rings (Dabiri et al., 2010; Herschlag and

Miller, 2011), where viscous effects become less important. At these larger spatial and temporal scales (where $Re \gg 1$), Stokes solutions for vortex rings become less applicable (Katija, unpublished data), and inviscid solutions (i.e., Hills spherical vortex; Batchelor, 1967) more so. This dependence on body size, power stroke duration, and travel distance suggests a continuous spectrum, rather than a binary choice, for the applicability of vortex ring models. Therefore, instead of sharp transitions where one impulsive viscous vortex ring model is applicable and not the other, the flow field more likely resembles both impulsive viscous vortex ring models to varying degrees. For example, although we conclude that swimming by ∼1 mm velar diameter *S. tubulosa* more closely resembles an impulsive Stokeslet, the non-zero vorticity field bounding the medusa's body during the contraction phase (Fig. 4) would suggest that the flow field is somewhere between an impulsive stresslet and impulsive Stokeslet. An additional metric (Test 2) provided further evidence that the flow field is better represented by an impulsive Stokeslet.

Significance to aquatic environments

[46] In order to understand complex interactions of organisms living in their natural, aquatic environment, mechanisms and behaviors relating to predation, survival, and their overall ecology need to be studied. Throughout its life cycle, an organism utilizes different swimming strategies and behaviors to feed, avoid predation, and reproduce (Yen and Strickler, 1996; Visser, 2001; Kiørboe, 2008). During these activities, organisms leave fluid signatures in their wake. Understanding how these fluid structures are manipulated and encountered by predators and prey can give an indication of an animal's success or fitness. We showed that small, jetting medusae are able to generate wake structures that are described in classical fluid dynamics by an impulsive Stokeslet. As an ambush feeding predator, the impulsive Stokeslet fluid signature exhibited by *S. tubulosa* is ecologically beneficial because they are able to swim to different regions of fluid undetected by their prey. In addition to *S. tubulosa*, a jetting medusae, these models can be extended to other small (on the order

of $\sim$1 mm), jetting animals in the viscous regime, including salps, squid paralarvae, and other species of medusae. These analytical models can then be used to elucidate complex animal-fluid interactions within animal aggregations (i.e., with multiple jetting units such as salp chains, doliolids, and siphonophores) and in turbulent environments.

References

Adrian, R. J., 1991. Particle–imaging techniques for experimental fluid–mechanics. Ann. Rev. Fluid Mech. 23, 261–304.

Afanasyev, Y. D., 2004. Wakes behind towed and self-propelled bodies: asymptotic theory. Phys. Fluids 16, 3235–3238.

Bartol, I. K., Krueger, P. S., Stewart, W. J., Thompson, J. T., 2009. Hydrodynamics of pulsed jetting in juvenile and adult brief squid *Lolliguncula brevis*: evidence of multiple jet 'modes' and their implications for propulsive efficiency. J. Exp. Biol. 212, 1889–1903.

Batchelor, G. K., 1967. An Introduction to Fluid Dynamics. Cambridge University Press, New York.

Blough, T., Colin, S. P., Costello, J. H., Marques, A. C., 2011. Ontogenetic changes in the bell morphology and kinematics and swimming behavior of rowing medusae: the special case of the Limnomedusa *Liriope tetraphylla*. Biol. Bull. 220, 6–14.

Catton, K. B., Webster, D. R., Yen, J., 2012. The effect of fluid viscosity, habitat temperature, and body size on the flow disturbance of *Euchaeta*. Limnol. Oceanogr. Fluids Env. 2, 80–92.

Colin, S. P., Costello, J. H., 2002. Morphology, swimming performance and propulsive mode of six co–occurring hydromedusae. J. Exp. Bio. 205, 427–437.

Colin, S. P., Costello, J. H., Klos, E., 2003. In situ swimming and feeding behavior of eight co-occurring hydromedusae. Mar. Ecol. Prog. Ser. 253, 305–309.

Costello, J. H., Colin, S. P., Dabiri, J. O., 2008. Constraints and consequences in medusan evolution. Invert. Biol. 127, 265–290.

Dabiri, J. O., Colin, S. P., Costello, J. H., 2006. Fast–swimming hydromedusae exploit velar kinematics to form an optimal vortex wake. J. Exp. Biol. 209, 2025–2033.

Dabiri, J. O., Colin, S. P., Costello, J. H., Gharib, M., 2005. Flow patterns generated by oblate medusan jellyfish: Field measurements and laboratory analyses. J. Exp. Biol. 208 (7), 1257–1265.

Dabiri, J. O., Colin, S. P., Katija, K., Costello, J. H., 2010. A wake-based correlate of swimming performance and foraging behavior in seven co-occurring jellyfish species. J. Exp. Biol. 213, 1217–1225.

Daniel, T. L., 1983. Mechanics and energetics of medusan jet propulsion. Can. J. Zool. 61, 1406–1420.

Daniel, T. L., 1985. Cost of locomotion: unsteady medusan swimming. J. Exp. Biol. 119, 149–164.

Eisenhauer, J. G., 2003. Regression through the origin. Teach. Stat. 25 (3), 76–80.

Feitl, K. E., Millett, A. F., Colin, S. P., Dabiri, J. O., Costello, J. H., 2009. Functional morphology and fluid interactions during early development of the scyphomedusa *Aurelia aurita*. Biol. Bull. 217, 283–291.

Guasto, J. S., Rusconi, R., Stocker, R., 2012. Fluid mechanics of planktonic microorganisms. Annu. Rev. Fluid Mech. 44, 373–400.

Herschlag, G., Miller, L., 2011. Reynolds number limits for jet propulsion: A numerical study of simplified jellyfish. J. Theor. Biol. 285, 84–95.

Jiang, H., Kiørboe, T., 2011a. The fluid dynamics of swimming by jumping in copepods. J. Roy. Soc. Interface 8, 1090–1103.

Jiang, H., Kiørboe, T., 2011b. Propulsion efficiency and imposed flow fields of a copepod jump. J. Exp. Biol. 214, 476–486.

Jiang, H., Meneveau, C., Osborn, T. R., 1999. Numerical study of the feeding current around a copepod. J. Plankton Res. 21, 1391–1421.

Jiang, H., Meneveau, C., Osborn, T. R., 2002. The flow field around a freely swimming copepod in steady motion: Part II numerical simulation. J. Plankton Res. 24, 191–213.

Jiang, H., Strickler, J. R., 2007. Copepod flow modes and modulation: a modeling study of the water currents produced by an unsteadily swimming copepod. Phil. Trans. Roy. Soc. B 362, 1959–1971.

Kiørboe, T., 2008. A mechanistic approach to plankton ecology. Princeton University Press, Princeton, NJ.

Kiørboe, T., Andersen, A., Langlois, V. J., Jakobsen, H. H., 2010a. Unsteady motion: escape jumps in planktonic copepods, their kinematics and energetics. J. Roy. Soc. Interface 7, 1592–1602.

Kiørboe, T., Jiang, H., Colin, S. P., 2010b. Danger of zooplankton feeding: the fluid signal generated by ambush-feeding copepods. Proc. Roy. Soc. B 277, 3229–3237.

Lighthill, M. J., 1975. Mathematical biofluiddynamics. SIAM, Philadelphia.

Lipinski, D., Mohseni, K., 2009. Flow structures and fluid transport for the hydromedusae *Sarsia tubulosa* and *Aequorea victoria*. J. Exp. Biol. 212, 2436–2447.

McHenry, M. J., Jed, J., 2003. The ontogenetic scaling of hydrodynamics and swimming performance in jellyfish (*Aurelia aurita*). J. Exp. Biol. 206, 4125–4137.

Murphy, D. W., Webster, D. R., Yen, J., 2012. A high-speed tomographic PIV system for measuring zooplanktonic flow. Limnol. Oceanogr. Methods 10, 1096–1112.

Sahin, M., Mohseni, K., Colin, S. P., 2009. The numerical comparison of flow patterns and propulsive performances for the hydromedusae *Sarsia tubulosa* and *Aequorea victoria*. J. Exp. Biol. 212, 2656–2667.

Turner, M. E., 1960. Straight line regression through the origin. Biometr. 16 (3), 483–485.

Visser, A. W., 2001. Hydrodynamic signals in the plankton. Mar. Ecol. Prog. Ser. 222, 1–24.

Weston, J., Colin, S. P., Costello, J. H., Abbott, E., 2009. Changing form and function during development in rowing hydromedusae. Mar. Ecol. Prog. Ser. 374, 127–134.

Willert, C. E., Gharib, M., 1991. Digital particle image velocimetry. Exp. Fluids 10 (4), 181–193.

Yen, J., Strickler, J. R., 1996. Advertisement and concealment in the plankton: What makes a copepod hydrodynamically conspicuous? Invertebr. Biol. 115, 191–205.

Tables

1 Summary of kinematic results for 11 data sets of swimming *Sarsia tubulosa* with ∼1 mm velar diameters. These data represent the values for relaxed velar diameter, bell height, bell width, contraction duration, and the distance traveled during a single swimming cycle. The Reynolds number (Re) is found where the characteristic length and velocity scales correspond to the relaxed velar diameter and maximum swimming speed, respectively. The average value and standard deviation of all parameters are shown.

2 Summary of measured ($I_{measured}$ and $M_{measured}$) and fitted results (I_{fitted}, M_{fitted}, and A_{sep}) and corresponding root mean squared error (RMSE) values for 11 data sets of ∼1 mm velar diameter *S. tubulosa*. As discussed in the Analytical Methods section, these values are used in two separate tests to determine whether the flow generated by ∼1 mm velar diameter *S. tubulosa* can be represented by an impulsive Stokeslet or impulsive stresslet viscous vortex ring model. The RMSE values associated with M_{fitted} and I_{fitted} are obtained by fitting the decay of fluid circulation (Γ, units of mm^2 s^{-1}); RMSE values for A_{sep} are obtained by fitting the average separation of vorticity maximum and minimum and velocity stagnation points with units of mm.

3 Summary of swimming behavior and impulsive vortex ring model of *S. tubulosa* and five different species of copepods: *Oithona davisae*, *Acartia tonsa*, *Calanus finmarchicus*, *Euchaeta rimana*, and *Euchaeta elongata* (Kiørboe et al., 2010a; Jiang and Kiørboe, 2011b,a; Murphy et al., 2012; Catton et al., 2012). The body size scale corresponds to the velar diameter and prosome length for *S. tubulosa* and copepods, respectively. The power stroke duration (t_{stroke}) corresponds to the contraction time duration of *S. tubulosa*. The distance traveled during a swimming cycle (d_{jump}) and maximum swimming speed (U_{max}), and maximum fluid circulation in the wake vortex (Γ_{max}) are shown in columns six, seven, and eight. The ninth column corresponds to the value for the strengths of the impulsive Stokeslet and stresslet vortex model, I and M, respectively. Values obtained from Kiørboe et al. (2010a) are indicated by a single asterisk; values obtained from a numerical model are indicated by a double asterisk.

Table 1. Summary of kinematic results for 11 data sets of swimming *Sarsia tubulosa* with ∼1 mm velar diameters. These data represent the values for relaxed velar diameter, bell height, bell width, contraction duration, and the distance traveled during a single swimming cycle. The Reynolds number (Re) is found where the characteristic length and velocity scales correspond to the relaxed velar diameter and maximum swimming speed, respectively. The average value and standard deviation of all parameters are shown.

Data set	Relaxed Velar Diameter (mm)	Bell Height (mm)	Bell Width (mm)	Time of Contraction (s)	Distance Traveled (mm)	Maximum Speed (mm s^{-1})	Reynolds Number
101107–13	1.3	1.3	1.7	0.10	1.1	14.5	14
101107–15	1.1	1.2	1.7	0.07	1.5	20.1	16
101107–21	1.2	1.0	1.6	0.10	1.6	13.0	12
101107–22	1.3	1.2	1.8	0.09	1.2	15.6	15
101117–4	1.1	1.9	1.9	0.08	1.4	10.9	9
101121–1a	1.2	1.7	1.9	0.08	2.2	21.5	19
101121–1b	1.2	1.7	1.9	0.08	2.5	22.6	20
101121–3	1.2	1.3	1.8	0.07	1.0	15.0	14
111129–1	1.0	1.1	1.3	0.10	2.9	20.4	15
111129–2	1.1	1.3	1.6	0.10	2.9	23.8	20
111129–3	1.1	1.3	1.4	0.09	2.2	19.8	17
Average ± Std Dev	1.2 ± 0.1	1.3±0.2	1.6±0.2	0.09 ± 0.01	1.9 ± 0.7	17.9 ± 4.3	15 ± 3

Table 2. Summary of measured ($I_{measured}$ and $M_{measured}$) and fitted results (I_{fitted}, M_{fitted}, and A_{sep}) and corresponding root mean squared error (RMSE) values for 11 data sets of ∼1 mm velar diameter *S. tubulosa*. As discussed in the Analytical Methods section, these values are used in two separate tests to determine whether the flow generated by ∼1 mm velar diameter *S. tubulosa* can be represented by an impulsive Stokeslet or impulsive stresslet viscous vortex ring model. The RMSE values associated with M_{fitted} and I_{fitted} are obtained by fitting the decay of fluid circulation (Γ, units of mm^2 s^{-1}); RMSE values for A_{sep} are obtained by fitting the average separation of vorticity maximum and minimum and velocity stagnation points with units of mm.

Data set	$I_{measured}$ (mm^4 s^{-1})	I_{fitted} (mm^4 s^{-1})	RMSE (mm^2 s^{-1})	$M_{measured}$ (mm^5 s^{-1})	M_{fitted} (mm^5 s^{-1})	RMSE (mm^2 s^{-1})	A_{sep}	RMSE (mm)
101107–13	27.49	47.51	0.067	30.34	91.98	0.067	1.56	1.40×10^{-3}
101107–15	38.66	39.41	0.052	56.59	74.49	0.052	1.59	7.35×10^{4}
101107–21	18.67	28.66	0.168	29.41	35.71	0.170	1.73	8.94×10^{4}
101107–22	30.93	27.73	0.128	36.88	49.42	0.128	1.61	9.80×10^{4}
101117–4	39.98	54.46	0.192	56.63	96.22	0.187	2.04	9.89×10^{4}
101121–1a	68.60	59.11	0.578	152.95	81.34	0.577	1.38	6.66×10^{4}
101121–1b	72.11	65.35	0.116	178.83	75.58	0.116	1.57	1.00×10^{3}
101121–3	31.73	31.00	0.042	32.86	114.60	0.042	1.14	6.06×10^{4}
111129–1	19.34	39.17	0.163	55.95	59.30	0.163	2.05	1.10×10^{3}
111129–2	39.15	56.48	0.150	114.26	74.10	0.150	1.98	8.92×10^{4}
111129–3	28.15	38.41	0.128	61.70	50.55	0.128	1.71	5.62×10^{4}
Average ± Std Dev	37.71 ± 17.67	44.30 ± 13.06	0.16±0.15	73.31 ± 51.85	73.03 ± 23.12	0.16±0.15	1.67 ± 0.28	$8.93 \times 10^{-4} \pm 2.44 \times 10^{-4}$

Table 3. Summary of swimming behavior and impulsive vortex ring model of *S. tubulosa* and five different species of copepods: *Oithona davisae*, *Acartia tonsa*, *Calanus finmarchicus*, *Euchaeta rimana*, and *Euchaeta elongata* (Kiørboe et al., 2010a; Jiang and Kiørboe, 2011b,a; Murphy et al., 2012; Catton et al., 2012). The body size scale corresponds to the velar diameter and prosome length for *S. tubulosa* and copepods, respectively. The power stroke duration (t_{stroke}) corresponds to the contraction time duration of *S. tubulosa*. The distance traveled during a swimming cycle (d_{jump}) and maximum swimming speed (U_{max}), and maximum fluid circulation in the wake vortex (Γ_{max}) are shown in columns six, seven, and eight. The ninth column corresponds to the value for the strengths of the impulsive Stokeslet and stresslet vortex model, I and M, respectively. Values obtained from Kiørboe et al. (2010a) are indicated by a single asterisk; values obtained from a numerical model are indicated by a double asterisk.

Organism	Swimming Behavior	Impulsive Model	Body Size (mm)	t_{stroke} (ms)	d_{jump} (mm)	U_{max} (mm s^{-1})	Γ_{max} (mm^2 s^{-1})	Fitted Impulsive Model Strength	Reference
O. davisae	repos. jump	stresslet	0.3	7	0.4	42			Jiang and Kiørboe (2011a)
O. davisae	escape		0.3	5	0.8	198			Kiørboe et al. (2010a)
A. tonsa	escape	stokeslet	0.7	7	7.2	333	31	I=19 mm^4 s^{-1**}	Jiang and Kiørboe (2011b)
A. tonsa	escape		0.7	4	1.9	378			Kiørboe et al. (2010a)
A. tonsa	repos. jump	stresslet	1.1	12	3.0	158	22	M=51 mm^5 s^{-1**}	Jiang and Kiørboe (2011b)
S. tubulosa	escape	stokeslet	1.2	90	1.9	18	112	I=44 mm^4 s^{-1}	Current
C. finmarchicus	escape, mult.	stresslet	2.1	10*		479	40	M=78 mm^5 s^{-1}	Murphy et al. (2012)
C. finmarchicus	escape		2.4	11	8.0	634			Kiørboe et al. (2010a)
C. finmarchicus	escape, mult.	stokeslet	3.0	12	66.2	756	97	I=2116 mm^4 s^{-1**}	Jiang and Kiørboe (2011b)
E. rimana	escape	stresslet	2.5			314	61	M=61 mm^5 s^{-1}	Catton et al. (2012)
E. elongata	escape	stresslet	3.4			276	93	M=93 mm^5 s^{-1}	Catton et al. (2012)

TABLES

Figures

1 Diagram representing the impulsive Stokeslet and impulsive stresslet models. (A) A swimming jellyfish traveling in the positive x-direction generates a jet directed in the negative x-direction. (B) Before swimming, the body's center of mass is located at the origin, and after swimming forward in the x-direction (position denoted by gray-dashed circle), vorticity surrounding the body (body-bound vorticity) and in the wake (wake vorticity) is generated. Red and blue patches represent positive and negative vorticity, respectively. (C) The impulsive Stokeslet model represents the wake as a single point momentum source at the origin, pointed in the opposite direction of travel (blue arrow). (D) The impulsive stresslet model represents the overall flow as two point momentum sources on the x-axis separated by a distance ϵ, pointed in opposite directions: one force pointed in the direction of travel (red arrow) and the other pointed opposite the direction of travel (blue arrow). Due to flow axisymmetry, only a meridian plane is shown in panels B-D.

2 Characteristic velocity (A) and vorticity (B) fields generated 0.52 s after the start of muscle contraction by ∼1 mm velar diameter *Sarsia tubulosa* (data set 111129–2). The black asterisks indicate the position of the velocity stagnation points and the vorticity minimum and maximum in panels A and B, respectively. The minimum vorticity contour level corresponds to -20 and 20 s^{-1} and the interval between contour lines is 20 s^{-1}. For clarity, the velocity and vorticity fields upstream of the velar exit are not shown.

3 Smoothed kinematic results of ∼1 mm *S. tubulosa* (data set 111129–2) velar diameter (left vertical axis; black, solid line), bell height (left vertical axis; black, dashed line), and swimming speed (right vertical axis; gray, solid line) derived from high-speed image capture of a single swimming cycle. The contraction phase starts at $t = 0$ s and the relaxation phase starts (and the contraction phase ends) at $t = 0.08$ s.

4 Representative velocity and vorticity fields of ∼1 mm velar diameter *S. tubulosa* (data set 101121–3). Black arrows indicate speed and direction of fluid in the region; red and blue contours indicate positive and negative vorticity, respectively. The time between each frame varies from 0.04, 0.05, and 0.1 s. The first panel (at $t = 0.025$ s) shows the velocity and vorticity field at the start of the contraction phase. The final panel (at $t = 0.215$ s) corresponds to the end of the relaxation phase.

5 The time-varying fluid circulation (left vertical axis, black dots) relative to the smoothed velar diameter (right vertical axis; solid, gray line) during a single swimming cycle for ∼1 mm velar diameter *S. tubulosa* (data set 101117–4). The gray, dashed line shows the nonlinear fit for the theoretical solution of an impulsive Stokeslet. The error bars represent the standard deviation between both values of circulation derived from the positive and negative values of vorticity.

6 Comparison between measured and fitted values of the strength of the impulsive Stokeslet (I, panel A) and stresslet (M, panel B), which is based on animal swimming kinematics and the decay of fluid circulation results. The solid line indicates the linear trend for each viscous vortex ring model. The R-squared values for the impulsive Stokeslet and impulsive stresslet models are 0.93 and 0.65, respectively.

7 Separation of vorticity maximum and minimum from the velocity stagnation points in the wake of a representative 1 mm velar diameter *S. tubulosa* (data set 101121–3). (A) Tracks of vorticity maximum/minimum and velocity stagnation points are indicated by circles and asterisks, respectively. The positions in time of these points are indicated by a sliding grayscale: initial, intermediary, and final positions correspond to light gray, gray, and black markers, respectively. (B) Average values of separation between the vorticity maximum and minimum and the velocity stagnation points in the animal's wake varies with time. The regression curve (black line) is fitted by $\Delta(t) = A_{sep}\sqrt{\nu\,(t - t_0)}$, where A_{sep} is 1.71, and the average for all ∼1 mm velar diameter cases is 1.67 (Table 2).

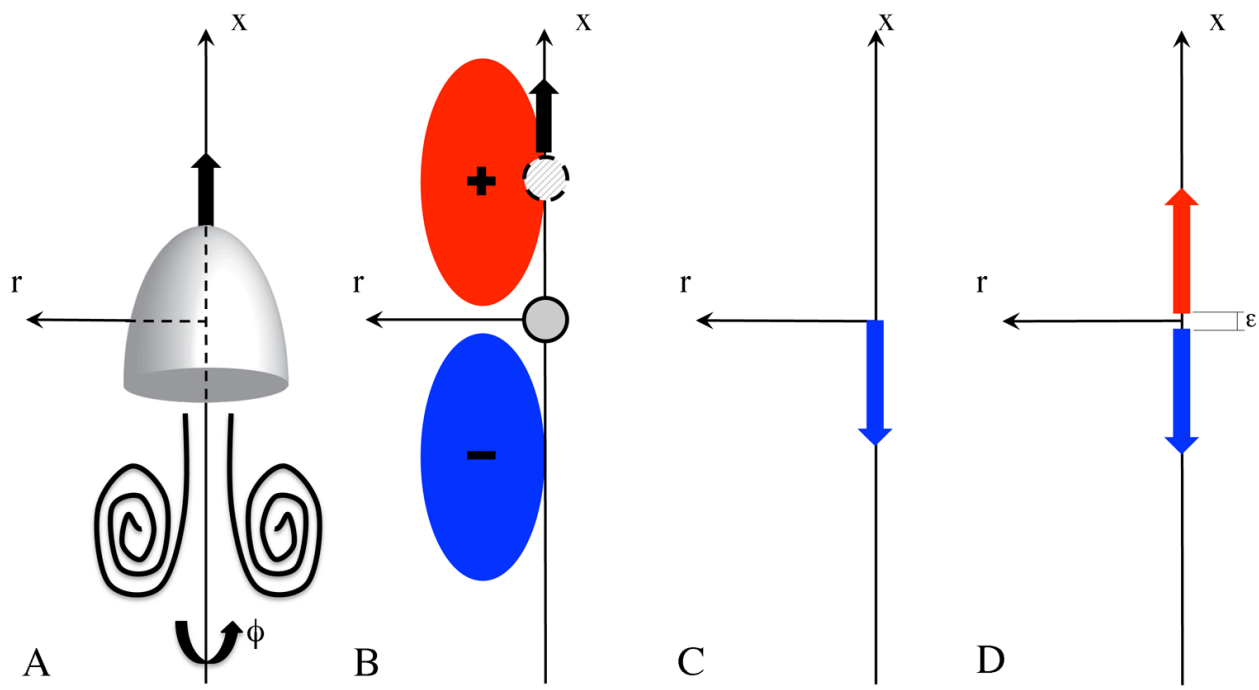

Fig. 1

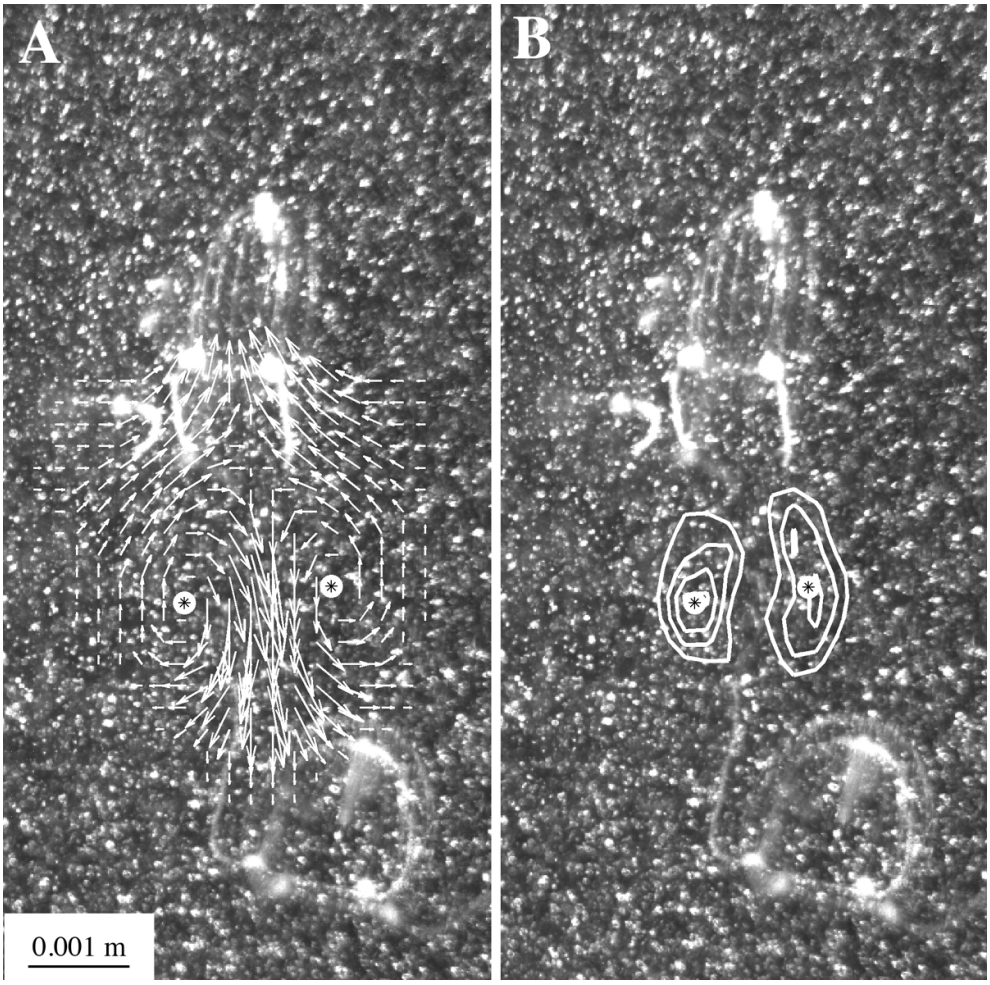

Fig. 2

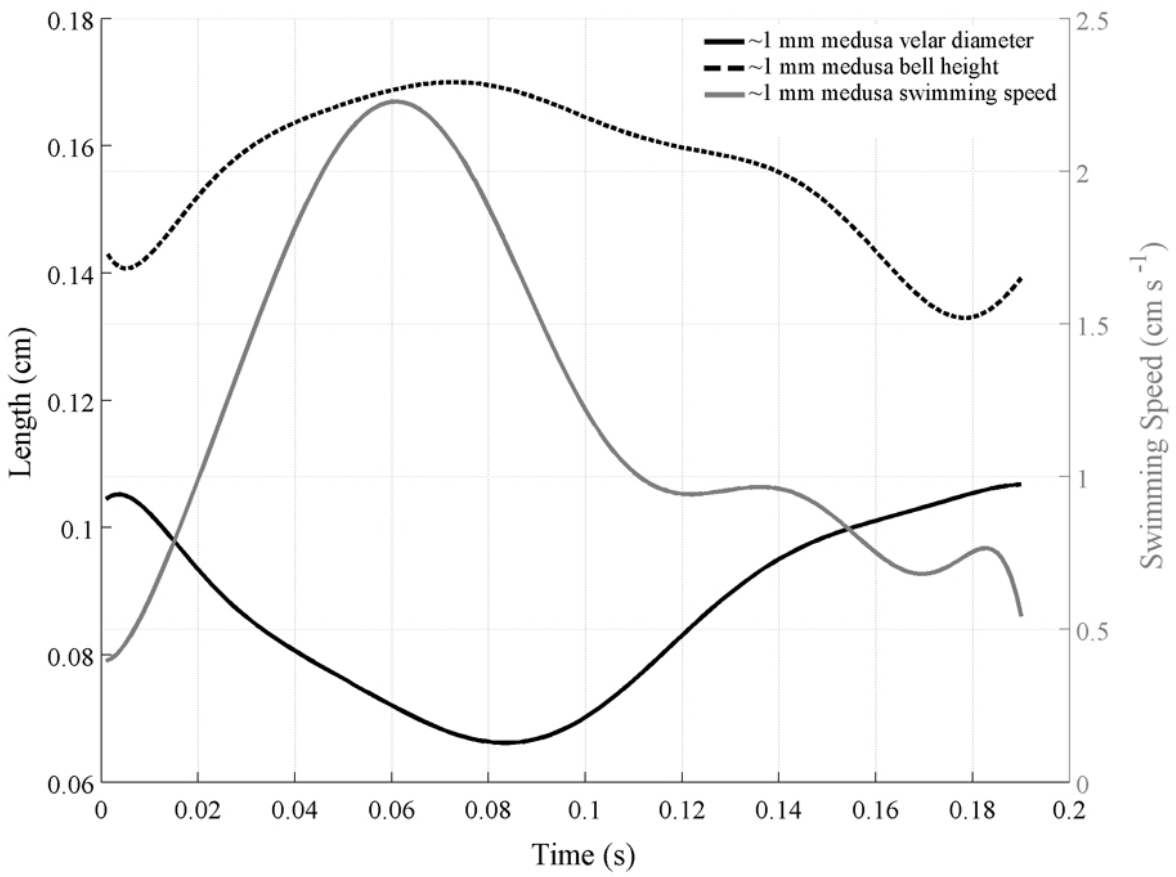
~1 mm medusa velar diameter
~1 mm medusa bell height
~1 mm medusa swimming speed
Length (cm)
Swimming Speed (cm s -1)
Time (s)
0.18
0.16
0.14
0.12
0.1
0.08
0.06
2.5
2
1.5
1
0.5
0
0
0.02
0.04
0.06
0.08
0.1
0.12
0.14
0.16
0.18
0.2

Fig. 3

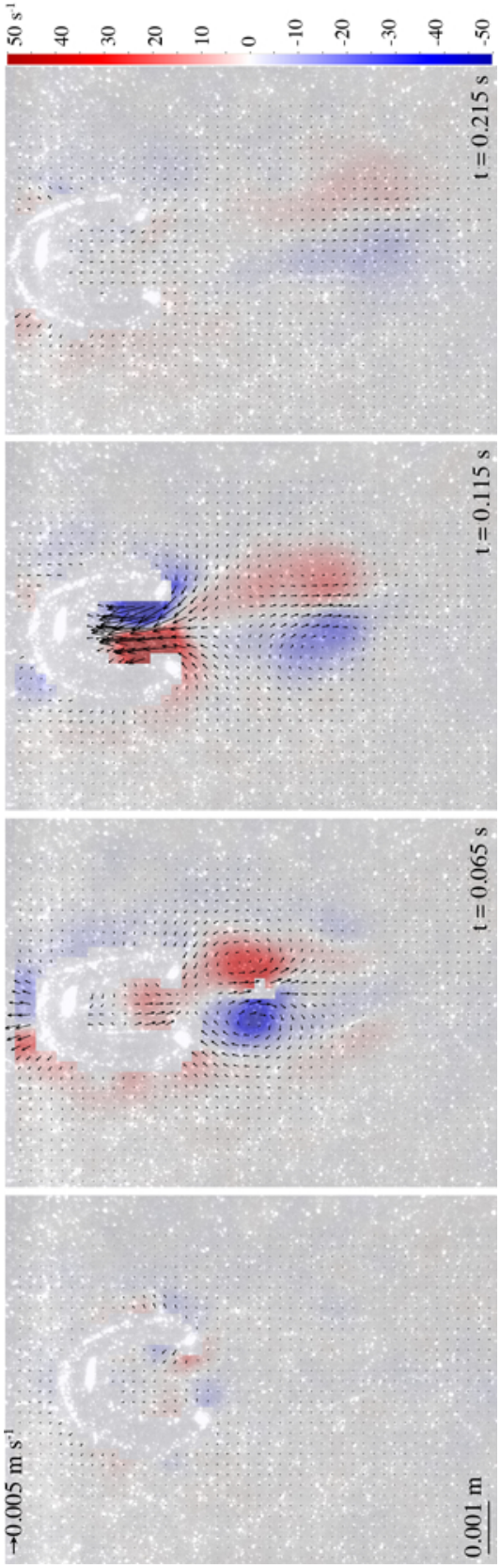
50 s⁻¹
40
30
20
10
0
-10
-20
-30
-40
-50
t = 0.215 s
t = 0.115 s
t = 0.065 s
→0.005 m s⁻¹
0.001 m

Fig. 4

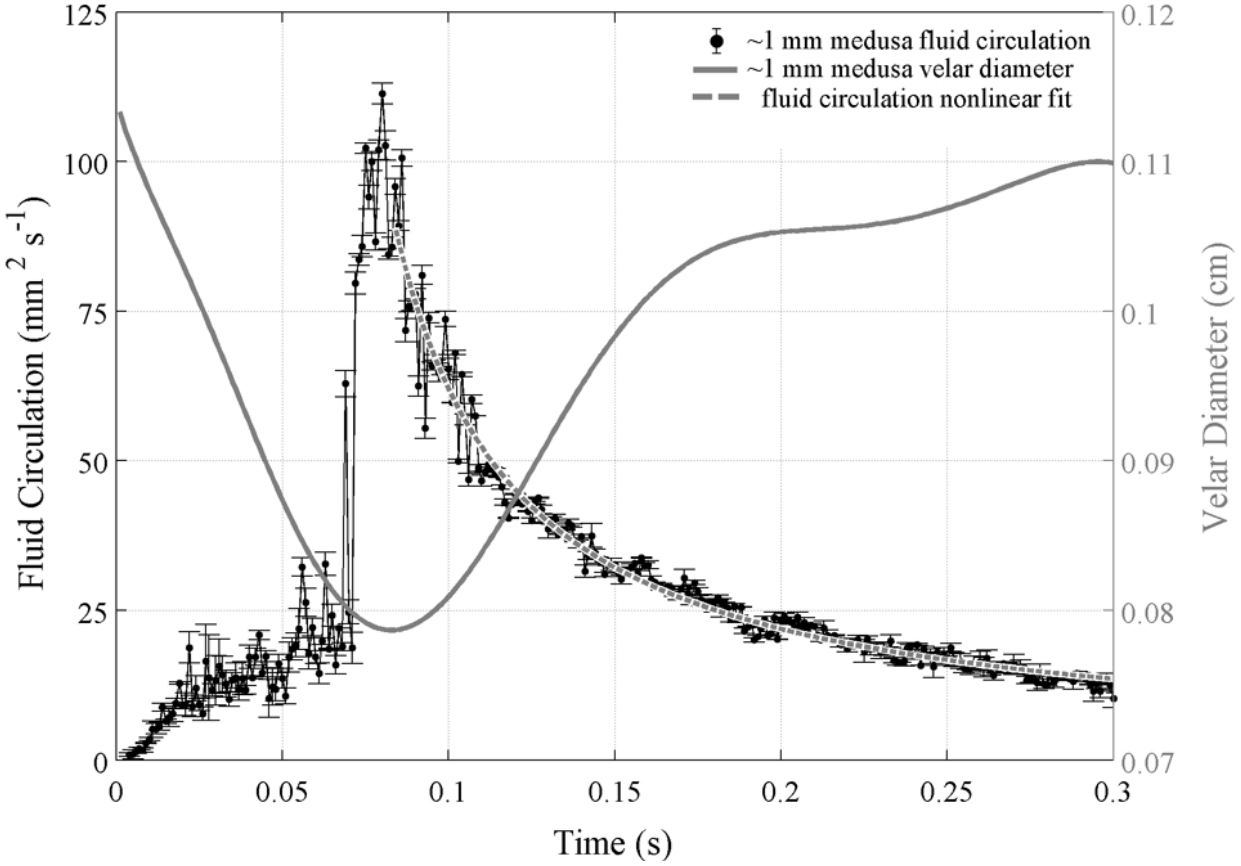
~1 mm medusa fluid circulation
~1 mm medusa velar diameter
fluid circulation nonlinear fit
Fluid Circulation (mm 2 s-1)
Velar Diameter (cm)
Time (s)
125
100
75
50
25
0
0.12
0.11
0.1
0.09
0.08
0.07
0
0.05
0.1
0.15
0.2
0.25
0.3

Fig. 5

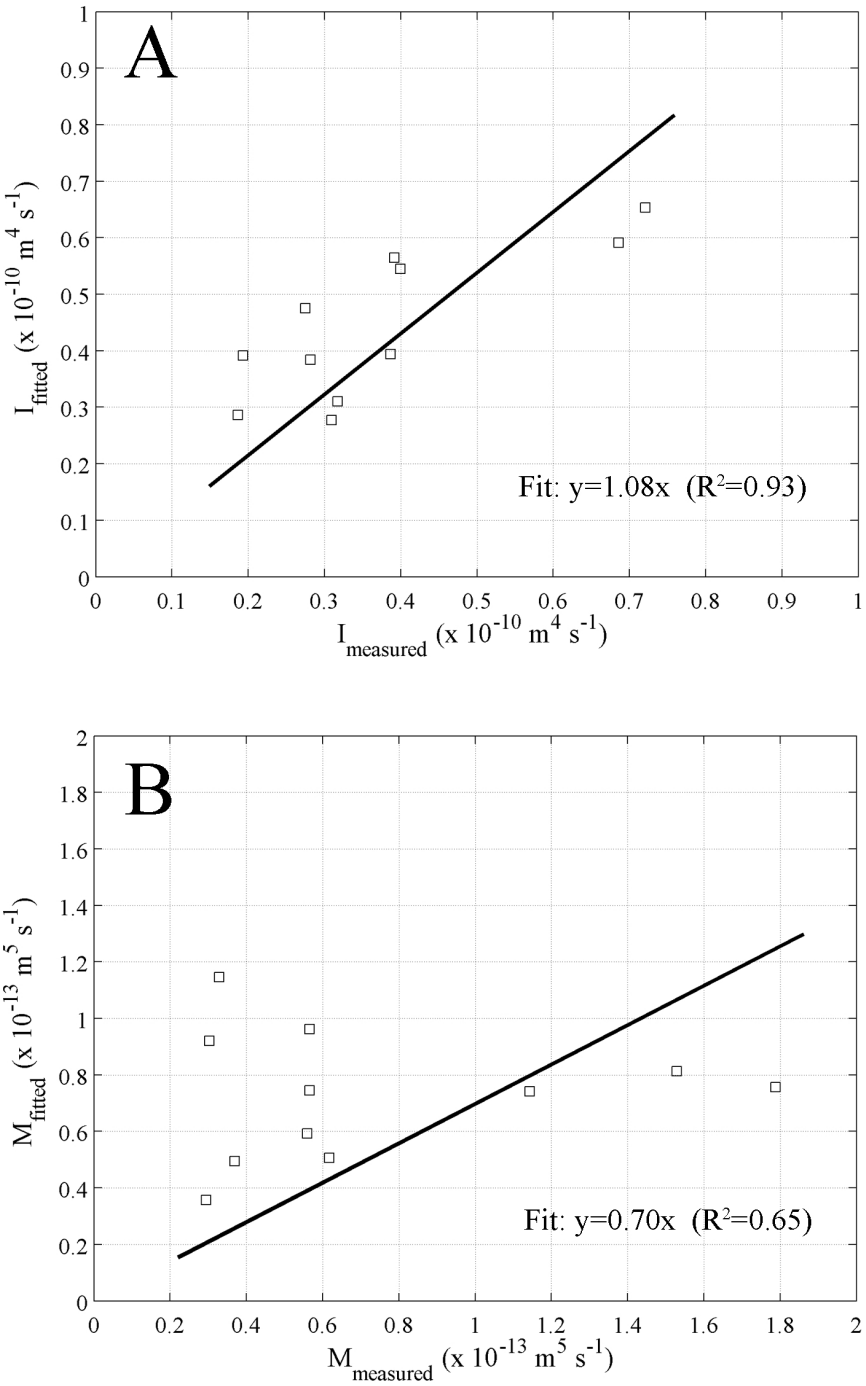
A
Fit: y=1.08x (R²=0.93)
I_fitted (x 10^-10 m^4 s^-1)
I_measured (x 10^-10 m^4 s^-1)
B
Fit: y=0.70x (R²=0.65)
M_fitted (x 10^-13 m^5 s^-1)
M_measured (x 10^-13 m^5 s^-1)

Fig. 6

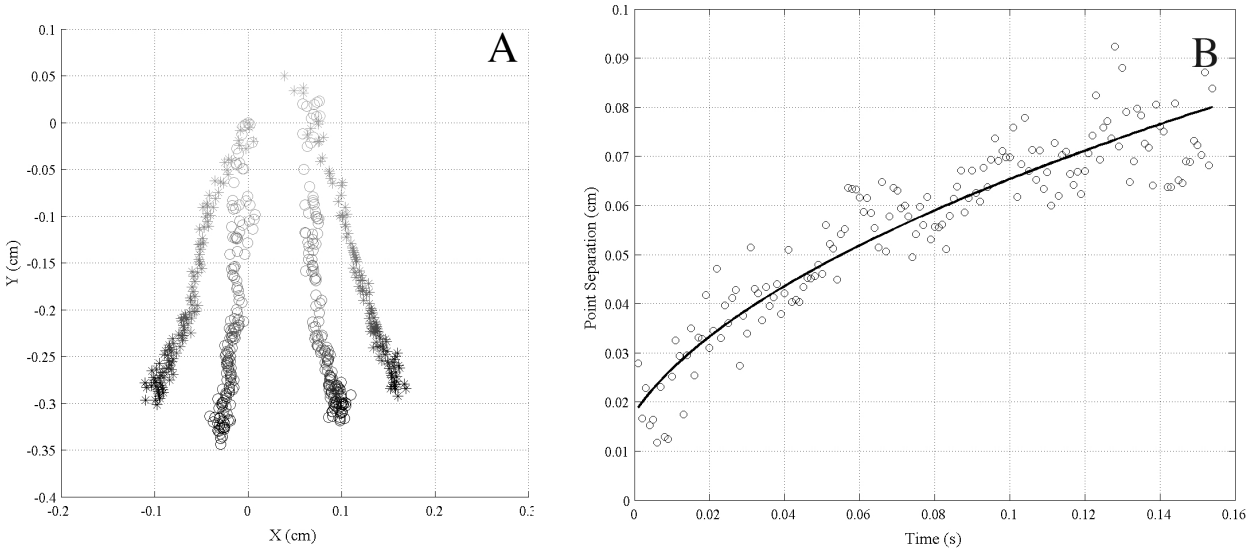

Fig. 7